

Article

**Size Effects on the Desorption of O from AuO/Au  
Nanoparticles Supported on SiO: A TPD Study**

Luis K. Ono, and Beatriz Roldan Cuenya

*J. Phys. Chem. C*, **2008**, 112 (47), 18543-18550 • Publication Date (Web): 04 November 2008

Downloaded from <http://pubs.acs.org> on November 21, 2008

**More About This Article**

Additional resources and features associated with this article are available within the HTML version:

- Supporting Information
- Access to high resolution figures
- Links to articles and content related to this article
- Copyright permission to reproduce figures and/or text from this article

[View the Full Text HTML](#)

# Size Effects on the Desorption of O<sub>2</sub> from Au<sub>2</sub>O<sub>3</sub>/Au<sup>0</sup> Nanoparticles Supported on SiO<sub>2</sub>: A TPD Study

Luis K. Ono and Beatriz Roldan Cuenya\*

Department of Physics, University of Central Florida, Orlando, Florida 32816

Received: July 23, 2008; Revised Manuscript Received: September 8, 2008

This article contains an in-depth study of the kinetics of O<sub>2</sub> desorption from preoxidized size-selected gold nanoparticles (NPs) of average size  $\sim 1.5$  and  $\sim 5$  nm synthesized by micelle encapsulation and supported on SiO<sub>2</sub>. Thanks to the narrow NP size distributions achieved using our preparation route, information on the effect of the nanoparticle size on the reaction kinetics could be obtained by temperature programmed desorption (TPD). In addition, the validity of different TPD analysis methods (Redhead, heating rate variation, Arrhenius plots, and the complete analysis) to extract meaningful kinetic parameters on supported NPs is discussed. From the different analysis methods, activation energies for O<sub>2</sub> desorption of  $E_d = 1.3 \pm 0.2$  eV and  $1.7 \pm 0.1$  eV were obtained for the  $\sim 5$  and  $\sim 1.5$  nm Au NPs, respectively. These differences in the activation energies are directly related to the nanoparticle size and not to nanoparticle-support interactions.

## Introduction

A number of studies can be found in the literature<sup>1–9</sup> describing kinetic parameters of O<sub>2</sub> desorption from gold single crystal surfaces with different orientations after atomic oxygen exposure. On the basis of the analysis of temperature programmed desorption (TPD) data, a range of desorption energies ( $E_d = 1.0 - 1.5$  eV), first-order ( $\nu_1 = 8 \times 10^9$  s<sup>-1</sup> to  $6 \times 10^{13}$  s<sup>-1</sup>), and second-order pre-exponential factors ( $\nu_2 \sim 10^{13}$  ML<sup>-1</sup> s<sup>-1</sup>) have been reported.<sup>1,2,4,6,7</sup> These differences can be partially assigned to the different initial adsorbate coverages ( $\theta_0$ ) considered because the kinetic parameters may depend on  $\theta_0$ ,<sup>5,6</sup> as well as to limitations of the particular TPD analysis method employed. In addition, the kinetic parameters may depend on the specific gold surface terminations investigated. Distinct reaction orders (pseudo first order,  $n = 1$  and  $n = 2$ ) have been reported,<sup>1,2,4,6,8</sup>  $n = 1$  being the most commonly observed desorption order for gold single crystal surfaces. The apparent first-order dependence of the desorption rate with adsorbate coverage might be due to adsorbate interactions.<sup>8</sup> An alternative mechanism was suggested by Kim et al.<sup>6,7</sup> in which the conversion of oxidic gold species to chemisorbed atomic oxygen is the rate-determining step in O<sub>2</sub> desorption.

Fewer studies<sup>9,10</sup> are available on the reaction kinetics of O<sub>2</sub> desorption from more complex systems, such as supported Au NPs. The presence of different surfaces in such systems (the support surface and the Au NP surface) adds a degree of complexity to the analysis of TPD data. Little is known on how the particle size and nanoparticle-support interactions might affect the kinetics, and an open question is whether the kinetic parameters previously reported on gold single crystals with different surface terminations<sup>1–9,11</sup> can be compared to those obtained by TPD on Au NPs, where surface facets with different crystalline orientations are present.<sup>12</sup>

In the present study, we have used self-assembled size-selected Au NPs synthesized by micelle encapsulation and deposited on SiO<sub>2</sub> as model experimental system.<sup>10</sup> We have acquired a series of TPD spectra as a function of the heating

ramp ( $\beta$ ) and the initial atomic oxygen coverage ( $\theta_0$ ) to get insight into the kinetics of O<sub>2</sub> desorption. Thanks to our sample preparation route, we have been able to measure desorption parameters on much more monodispersed particle size distributions than previous studies and to find how such parameters change as a function of the particle size. Furthermore, the obtained experimental data permit us to evaluate the validity of different TPD analysis methods to extract reliable desorption energies and pre-exponential factors on supported NPs.

## Analysis Methods

Significant efforts have been dedicated in the past to the development of procedures to extract kinetic parameters from TPD spectra.<sup>13–17</sup> The starting point of all treatments is the desorption rate equation proposed by Polanyi and Wigner (PW)<sup>16,18,19</sup>

$$R = -\frac{d\theta}{dt} = -\frac{d\theta}{dT} \beta = \nu_n \theta^n \exp(-E_d/kT) \quad (1)$$

where  $\theta$  is the adsorbate coverage [in monolayer (ML) units],  $\beta$  is the heating rate,  $n$  is the desorption order,  $\nu_n$  is the pre-exponential factor,  $E_d$  is the desorption energy, and  $k$  is the Boltzmann constant.

The TPD analysis methods have been divided in two categories:<sup>20</sup> (i) integral methods including the Redhead<sup>15</sup> and Chan–Aris–Weinberg (CAW)<sup>13</sup> analysis, and (ii) differential methods<sup>20</sup> such as the leading edge analysis<sup>21</sup> and complete analysis.<sup>16,22</sup> The integral methods are based on the temperature at the desorption rate maximum ( $T_{\max}$ ), and/or peak half-widths, and assume coverage-independent values for  $n$ ,  $E_d$ , and  $\nu_n$ . As an example, the following expressions have been proposed by Redhead<sup>15</sup> to analyze first- (eq 2) and second-order (eq 3) desorption processes:

$$\frac{E_d}{kT_{\max}} = \ln\left(\frac{\nu_1 T_{\max}}{\beta}\right) - 3.64 \quad \text{for } n = 1 \quad (2)$$

$$\frac{E_d}{kT_{\max}^2} = \frac{2\theta_{\max}\nu_2}{\beta} \exp\left(-\frac{E_d}{kT_{\max}}\right) \quad \text{for } n = 2 \quad (3)$$

where  $\theta_{\max}$  is the adsorbate coverage at  $T = T_{\max}$ , and  $\theta_{\max} \approx \theta_0/2$ , with  $\theta_0$  being the initial surface coverage.

\* To whom correspondence should be addressed. E-mail: roldan@physics.ucf.edu.

The heating rate variation method (HRV) by Falconer and Madix<sup>17</sup> is considered suitable for determining the desorption energy without making any assumptions concerning the pre-exponential factor or specific reaction mechanisms. Following this method, eq 1 is differentiated with respect to temperature, and the second derivative is set equal to zero for the temperature of the maximum desorption rate:

$$\ln\left(\frac{\tilde{T}_{\max}^2}{\tilde{\beta}}\right) = \frac{E_d}{k} \cdot \frac{1}{T_{\max}} + \ln\left(\frac{\tilde{E}_d}{\tilde{k}\tilde{\nu}_n n \tilde{\theta}_{\max}^{n-1}}\right) \quad (4)$$

In eq 4, the tildes indicate normalization by the quantity's own units. This method is used to analyze a set of TPD spectra measured with different heating ramps for a constant initial coverage. Graphs of  $\ln(\tilde{T}_{\max}^2/\tilde{\beta})$  versus  $1/T_{\max}$  are constructed, and the desorption energy is extracted from the slope of the linear fit. No assumption of the desorption order  $n$  needs to be made in order to obtain  $E_d$ . The pre-exponential factor can be extracted from the intercept of the  $y$ -axis in eq 4. For first-order desorption processes,  $\nu_1$  does not depend on the coverage, whereas for  $n = 2$  the coverage at the desorption maximum,  $\theta_{\max}$ , is used to determine  $\nu_2$  from eq 4.

In the differential TPD analysis methods,  $(-d\theta/dt, T)$  pairs are used to generate Arrhenius plots [ $\ln(-d\theta/dt) - n \ln \theta$  versus  $1/T$ ] from which  $E_d$  and  $\nu_n$  can be obtained from the slope and  $y$  axis intercept of a single TPD spectrum, respectively, in cases where  $E_d$  and  $\nu_n$  are coverage independent, as seen in eq 5. This method should only be used to analyze systems with little adsorbate–adsorbate interactions and in general, when low adsorbate coverages are considered. Under these assumptions, the following equation applies:

$$\ln\left(-\frac{d\theta}{dt}\right) - n \ln \theta = \ln \nu_n - E_d/kT \quad (5)$$

However, if the kinetic parameters depend on  $\theta$ , the slope of the Arrhenius plot becomes more complicated. Terms including derivatives of  $E_d(\theta)$  and  $\nu_n(\theta)$  with respect to  $\theta$  appear, and eq 5 can only be used under certain circumstances:<sup>20</sup> (i)  $d\theta/d(1/T)$  is small, and (ii) the sum of the additional derivative terms is zero,  $1/kT[\partial E_d(\theta)/\partial\theta] = [\partial \ln \nu_n(\theta)/\partial\theta]$ . The second possibility is commonly known as the compensation effect,<sup>20,23–27</sup> in which  $E_d(\theta)$  and  $\nu_n(\theta)$  may vary with  $\theta$ , but the product  $\nu_n(\theta) \exp[-E_d(\theta)/kT]$  is nearly constant. It is not possible to know if such compensation effects will be present on a particular system a priori, and applying eq 5 to a single-TPD data set where this is not the case will result in erroneous  $E_d$  and  $\nu_n$  values.

A series of Arrhenius plots corresponding to different instantaneous adsorbate coverages can be used to extract more reliable information on the possible dependency of the kinetic parameters [ $E_d(\theta')$  and  $\nu_n(\theta')$ ] on the adsorbate coverage. This method was proposed by King et al.<sup>22</sup> and is known as the complete analysis. A similar differential method was developed by Taylor and Weinberg,<sup>14</sup> where Arrhenius plots from several TPD spectra are acquired as a function of the heating rate and coverage.

To extract the desorption order  $n$  from TPD measurements, desorption isotherms<sup>2,28</sup> are commonly used. For this analysis, a plot of  $\ln(-d\theta/dt)$  versus  $\ln \theta$  at a constant temperature is constructed. On the basis of eq 1, such a plot should yield a straight line with slope  $n$ , if  $E_d$  and  $\nu_n$  are coverage independent. In cases where  $E_d$  and  $\nu_n$  depend on  $\theta$ , a logarithmic differentiation of eq 1 with respect to the coverage at constant  $T$ , eq 6 reveals that the slope of the  $\ln(-d\theta/dt)$  versus  $\ln \theta$  plot will not provide the correct desorption order. Again, only when

compensation effects<sup>20,23–27</sup> are present, the last two terms in eq 6 can be neglected:

$$\text{slope} = \frac{\partial \ln(-d\theta/dt)}{\partial \ln \theta} \Big|_T = n + \frac{\partial \ln \nu_n(\theta)}{\partial \ln \theta} \Big|_T - \frac{1}{kT} \frac{\partial E_d(\theta)}{\partial \ln \theta} \Big|_T \quad (6)$$

Investigations by Ibbotson et al.<sup>24</sup> and Wittrig et al.<sup>25</sup> on the desorption order of H<sub>2</sub> on Ir(110) based on the slopes of  $\ln(-d\theta/dt)$  versus  $\ln \theta$  plots at constant temperatures revealed a desorption order equal to 2 for high desorption temperatures (i.e., low coverage) and much greater than 2 for high coverages, where stronger adsorbate interactions are expected. Because the dissociative adsorption of H<sub>2</sub> is expected on this system, the authors concluded that compensation effects may be responsible for the anomalous desorption order obtained when high adsorbate coverages were considered.

The ability of common TPD analysis methods (Redhead, CAW, HRV, and complete analysis) to provide accurate desorption energies and pre-exponential factors for a range of initial adsorbate coverages was tested by de Jong et al.<sup>28</sup> using a set of simulated TPD curves with known  $E_d(\theta)$  and  $\nu_n(\theta)$  values. The results of this test revealed the limitations of the integral methods. As an example, the CAW method only predicted the correct  $E_d$  at the zero-coverage limit. The HRV method by Falconer and Madix<sup>17</sup> was also found to fail when high coverages were considered. Reliable information over the entire coverage range was only obtained with the leading edge and complete analysis methods. However, one should keep in mind that the leading-edge and complete analysis methods require very good quality TPD data and the presence of nonoverlapping desorption sites, what is rarely the case for complex systems such as supported clusters. Experimental factors such as the presence of excessive noise in the low-temperature region (leading-edge), residual intensity in the high-temperature tail of the TPD spectra (due for example to limited pumping speed or redesorption from elements within the UHV system other than the sample), and possible uncertainties in the background subtraction will lead to incorrect estimations of the desorption parameters of real TPD data sets using these methods.

A second type of compensation effect was described by Nieskens et al.<sup>27</sup> and it is related to the collection of discrete data points in TPD measurements. A set of TPD spectra were simulated using dynamic Monte Carlo (DMC) calculations with an a priori known expression for the activation energy ( $E_d = 1 - 0.2\theta$  eV), considering coverage-dependent lateral adsorbate interactions and assuming a fixed pre-exponential factor ( $10^{14}$  s<sup>-1</sup>). Results from the complete analysis on these data showed a large scattering on the activation energies ( $\sim 0.7$  to 1.1 eV) and pre-exponential factors ( $\sim 5 \times 10^{12}$  to  $1 \times 10^{17}$  s<sup>-1</sup>) as well as a strong compensation effects as a function of the coverage. The authors concluded that even though the complete analysis was found to provide reliable kinetic parameters<sup>28,29</sup> based on continuous TPD curves calculated from the analytical expression in eq 1, its application to the analysis of real TPD data (discrete set of data points) might lead to a large scattering in the values of the kinetic parameter as a function of the coverage,  $\theta$ .

In this article, we have applied the HRV,<sup>14</sup> complete analysis,<sup>30</sup> and Redhead<sup>15</sup> methods, as well as simulations following the Wigner–Polanyi equation, to analyze experimental TPD spectra for O<sub>2</sub>-desorption from  $\sim 5$  and  $\sim 1.5$  nm Au NPs supported on SiO<sub>2</sub>. Our results will provide insight into the validity of these common analysis methods to extract kinetic

parameters from complex systems, where coverage-dependent adsorbate interactions are likely to be present.

## Experimental

Size-selected Au NPs were synthesized by inverse micelle encapsulation on polystyrene-block-poly(2-vinylpyridine) diblock copolymers [PS(x)-b-P2VP(y), Polymer Source Inc.].<sup>12</sup> Chloroauric acid (HAuCl<sub>4</sub>·3H<sub>2</sub>O) was used as metal seed. Different average NP sizes were obtained using two diblock-copolymers with distinct P2VP molecular weight (polymer head): PS(53000)-P2VP(43800) and PS(8200)-P2VP(8300). The micelles containing Au NPs were deposited onto naturally oxidized SiO<sub>2</sub>/Si(111) substrates by dip-coating at a speed of 1 μm/min. Subsequently, the samples were transferred into an ultrahigh vacuum system (UHV, SPECS GmbH) and the encapsulating polymer was removed via an O<sub>2</sub>-plasma treatment ( $P_{O_2} = 5.5 \times 10^{-5}$  mbar for 100 min) at 150 K. After this treatment, no residual polymeric carbon signal was detected by X-ray photoelectron spectroscopy (XPS). In addition, high resolution XPS measurements from the Au 4f core level region revealed the presence of Au<sup>0</sup> and Au<sup>3+</sup> compounds in these samples.<sup>10</sup> Further sample preparation details and morphology characterization are given in ref 10. The samples investigated here are identical to samples #1 (~5 nm Au NPs) and #3 (~1.5 nm) in ref 10.

The O<sub>2</sub> desorption TPD measurements were carried out in UHV with a system consisting of a differentially pumped quadrupole mass spectrometer (QMS, Hiden Analytical, HAL 301/3F) and electron-bombardment sample heating connected to a PID temperature controller (Eurotherm, 2048). The base pressure in this UHV chamber is  $1-2 \times 10^{-10}$  mbar. Prior to the TPD measurements, the polymer-free Au NPs were flash annealed to 700 K. This procedure served to decrease the residual gas background at high temperatures. No significant changes in the NP size distribution were observed after this treatment.<sup>10</sup> Subsequently, the samples were exposed to atomic oxygen at room temperature ( $P_{O_2} = 2.3 \times 10^{-5}$  mbar) during different time intervals from 10 s to 20 min. For the TPD studies, the samples were kept at RT during O<sub>2</sub> plasma exposure and subsequently, the samples were placed ~3 mm away from the mass spectrometer glass shield opening (5 mm aperture) and heating rates ( $\beta$ ) ranging from 0.1 to 5 K/s were used.

## Results and Discussion

**a) Heating Rate Variation (HRV).** Parts a and b of Figure 1 show a series of O<sub>2</sub> desorption spectra obtained from ~5 nm high Au NPs (sample #1) and ~1.5 nm NPs (sample #3) respectively as a function of the heating ramp ( $\beta$ ) from 0.1 to 5 K/s. These sizes correspond to the NPs investigated in ref 10. The samples were pre-exposed for 15 min to atomic oxygen produced by an O<sub>2</sub>-plasma source with an O<sub>2</sub> pressure of  $2.0 \times 10^{-5}$  mbar. The initial oxygen coverage was kept constant, and coverages of  $\theta_0 = 0.22 \pm 0.06$  monolayers (ML) for the 5 nm NPs and  $\theta_0 = 0.26 \pm 0.05$  ML for the ~1.5 nm NPs were obtained by integrating the second peak ( $\gamma$  in Figure 1) of the respective TPD desorption spectra. Note that in these studies  $\theta_0$  denotes the relative atomic oxygen coverage on gold, that is, a ML was defined as one oxygen atom per surface gold atom. Further details on the calculation of the adsorbate coverages are given below.

For both samples, a relatively small desorption peak appears at ~400 K ( $\sigma$  state), which was identified as O<sub>2</sub> desorption from the SiO<sub>2</sub> substrate,<sup>10</sup> as shown in Figure 1. In addition to the  $\sigma$  state, a clear desorption peak is observed at higher temperatures for the Au NP coated samples, labeled as state  $\gamma$ . As discussed

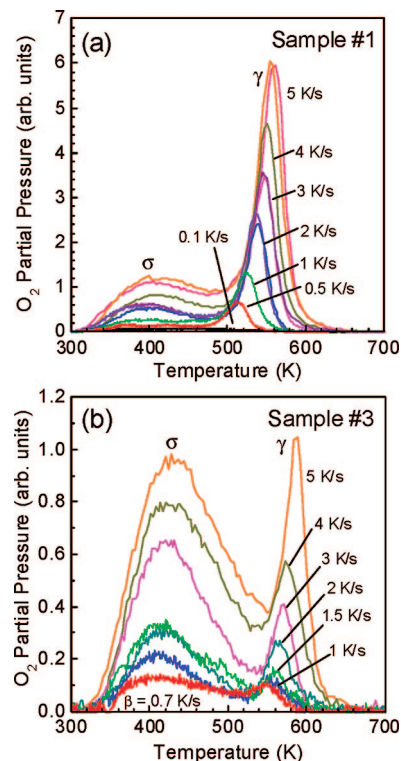


**Figure 1.** Series of O<sub>2</sub> TPD spectra obtained on (a) ~5 nm (sample #1) and (b) ~1.5 nm (sample #3) Au NPs deposited on SiO<sub>2</sub> for a constant initial oxygen coverage of 0.22 and 0.26 ML, respectively. The heating rate ( $\beta$ ) has been varied from 0.1 to 5 K/s.

in ref 10, this state can be attributed exclusively to O<sub>2</sub> desorption from our preoxidized Au NPs.

The adsorbate coverage in ML in our system can be estimated using morphology data obtained from AFM measurements on our samples. From the measured particle height distribution and NP areal density, and using the known near-hemispherical particle shape found in TEM measurements (not shown), we have calculated the total gold surface area for each sample. Assuming an areal density of gold surface atoms of  $\sim 2 \times 10^{15}$  atoms/cm<sup>2</sup> [a typical number for Au(110)<sup>2,9</sup>], the gold atomic density in our samples was found to be  $1.4 \times 10^{14}$  atoms/cm<sup>2</sup> (~5 nm NPs) and  $2.0 \times 10^{13}$  atoms/cm<sup>2</sup> (~1.5 nm NPs). It should be noted that these numbers are 1–2 orders of magnitude smaller than the gold surface densities calculated for continuous gold films due to the only partial gold coverage of the SiO<sub>2</sub> substrate. For each sample, a coverage of 1 ML is defined as one oxygen atom per gold surface atom. The temperature-dependent O<sub>2</sub> pressure detected by our mass spectrometer was converted to molecular flux in O<sub>2</sub> molecules per cm<sup>2</sup> per second using the gas effusion equation. Note that in this conversion one must use room temperature (298 K), rather than the sample temperature. Subsequently, these fluxes were converted to ML/s using the previously described definition of 1 ML, and taking into account the fact that each detected O<sub>2</sub> molecule corresponds to two oxygen atoms. All ML coverages were obtained from the integration of the second desorption peak ( $\gamma$  in Figure 1) because the first peak ( $\sigma$ ) originates from the SiO<sub>2</sub> substrate.

The desorption energy and pre-exponential factor of the  $\gamma$  peak have been obtained here using the HRV method.<sup>2,16,17</sup> As can be seen from eq 4, the activation energy for desorption can be obtained without making any assumptions on the desorption order. However, an assumption needs to be made on the desorption order if one intends to calculate the pre-exponential

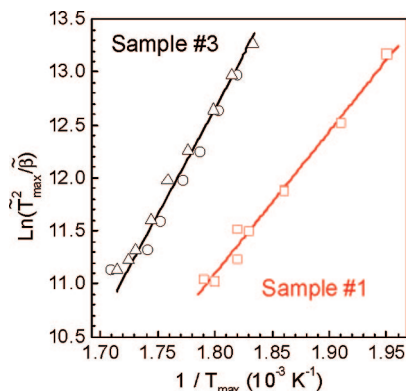


**Figure 2.**  $\ln(\tilde{T}_{\max}^2/\tilde{\beta})$  versus  $1/T_{\max}$  plots obtained from the heating rate variation data displayed in Figure 1. The data correspond to the  $O_2$  desorption state labeled as  $\gamma$ . Data from two Au NP/SiO<sub>2</sub> samples are shown: sample #1 ( $\sim 5$  nm height) and sample #3 ( $\sim 1.5$  nm height). The open squares correspond to the data obtained on sample #1, whereas the open circles and triangles correspond to two sets of measurements conducted on sample #3.

factor. Figure 2 shows the corresponding  $\ln(\tilde{T}_{\max}^2/\tilde{\beta})$  versus  $1/T_{\max}$  graphs for large ( $\sim 5$  nm high, sample #1) and small ( $\sim 1.5$  nm, sample #3) NPs. Using the HRV method, activation energies for  $O_2$  desorption of  $1.2 \pm 0.1$  and  $1.7 \pm 0.1$  eV were obtained for our large ( $\sim 5$  nm) and small ( $\sim 1.5$  nm) Au NPs, respectively. Throughout this article, the error bars indicated correspond to the statistical error resulting from the corresponding linear fits. It should be noted that these error margins are much smaller than the differences observed in activation energy with particle size. The activation energy obtained for the small NPs ( $\sim 1.5$  nm) using this method is very similar to the value of  $1.6 \pm 0.1$  eV reported in our earlier publication<sup>10</sup> based on the linear fit of the Arrhenius plot observed for  $n = 2$  in a single-TPD spectrum. The initial oxygen coverage on both samples was similar, with an average  $\theta_0 = 0.26$  ML on the  $\sim 1.5$  nm NPs in the HRV data, and 0.31 ML in the TPD spectrum of ref 10 ( $\beta = 5$  K/s) for an analogous sample. For the 5 nm NPs, the value for  $E_d$  obtained here is slightly larger than the value that we previously reported in ref 10 ( $1.0 \pm 0.1$  eV) due to a numerical error in the Arrhenius plot of the original manuscript<sup>10,31</sup> [Figure 9(c) in ref 10].

Assuming that the behavior of our large gold NPs (part a of Figure 1) follows first order kinetics, as has been indicated by some authors for certain oxygen coverages on bulk gold crystals,<sup>5–7</sup> we can obtain the pre-exponential factor for this system using the HRV method from the intercept with the y axis of the least-squares linear fit to the  $\ln(\tilde{T}_{\max}^2/\tilde{\beta})$  versus  $1/T_{\max}$  data. It should be noted that the desorption rate of  $O_2$  from bulk gold surfaces might display an apparent linear dependency on the adsorbate coverage due to adsorbate–adsorbate interactions or compensation effects.<sup>20,27</sup> Using  $n = 1$  in the HRV method and  $E_d = 1.2$  eV, a pre-exponential factor of  $1 \times 10^{10 \pm 1} \text{ s}^{-1}$  was obtained for our large nanoparticles ( $\sim 5$  nm). This value is slightly lower than what has been previously reported for bulk gold single crystals.<sup>4,6</sup> However, it should be emphasized that the desorption of  $O_2$  from Au NPs might be different from that of bulk gold surfaces due to a higher density of surface defects, on the NPs, the presence of facets with various crystal orientations,<sup>32</sup> additional particle-support interactions, and distinct surface phonons in the NPs<sup>33</sup> that could affect the desorption curve and the corresponding apparent pre-exponential factor.

In addition, second-order  $O_2$  desorption has also been reported for bulk gold systems.<sup>1,2</sup> If one considers that  $n = 2$  might

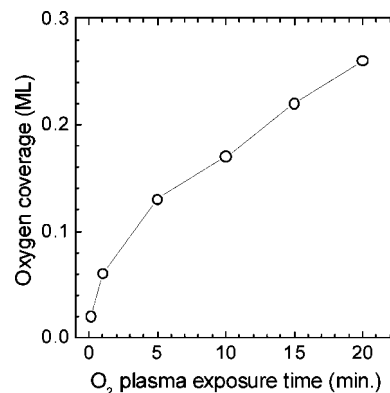


**Figure 3.** Oxygen uptake curve on  $\sim 5$  nm Au NPs (sample #1) after different room-temperature  $O_2$  plasma exposure times.

describe the behavior of our large Au NPs, the initial adsorbate coverage must be known in order to obtain the pre-exponential factor. For an oxygen coverage  $\theta_0$  of 0.22 ML ( $\theta_{\max} \approx 0.1$  ML) and assuming  $n = 2$ , a pre-exponential factor  $\nu_2$  of  $4 \times 10^{10 \pm 1} \text{ ML}^{-1} \text{ s}^{-1}$  was obtained for the  $\sim 5$  nm NPs from the HRV method. This value is lower than that previously reported by Gottfried et al.<sup>2</sup> for Au(110) ( $\sim 2 \times 10^{13} \text{ ML}^{-1} \text{ s}^{-1}$ ). For the small gold NPs ( $\sim 1.5$  nm), the Arrhenius plot of  $\ln(-d\theta/dt) - n \ln \theta$  versus  $1/T$  in Figure 9(d) of ref 10 indicated that the desorption of oxygen can be described by a second-order process. Thus, assuming  $n = 2$  and an initial O coverage on Au,  $\theta_0 = 0.26$  ML ( $\theta_{\max} \approx 0.1$  ML), a pre-exponential factor  $\nu_2$  of  $2 \times 10^{15 \pm 1} \text{ ML}^{-1} \text{ s}^{-1}$  was obtained from the HRV method for the  $\sim 1.5$  nm clusters. The resultant pre-exponential factor is in agreement with the value of  $7 \times 10^{14 \pm 1} \text{ ML}^{-1} \text{ s}^{-1}$  that was obtained previously on this sample from the Arrhenius plot of a single TPD spectrum [intercept with the y axis in Figure 9(d) in ref 10] for  $n = 2$ , after appropriate unit conversion.

**b) Complete Analysis: Coverage-Dependent  $O_2$  Desorption.** Previous studies on gold single crystals<sup>2,5,6</sup> have indicated that the kinetic parameters of  $O_2$  desorption from preoxidized gold surfaces may depend on the adsorbate coverage. To clarify this point, in addition to the heating rate dependent data, two sets of  $O_2$  TPD spectra with a constant heating ramp of 5 K/s were acquired on the 5 nm Au NPs (sample #1) and 1.5 nm Au NPs (sample #3) for a range of initial adsorbate coverages ( $\theta_0$ ). The evaluation of these experimental data has been carried out using the complete analysis method.<sup>16,28,30</sup> Figure 3 shows the oxygen uptake by Au NPs in sample #1 as a function of the oxygen plasma exposure time determined by the integration of the  $\gamma$  TPD peak using a heating ramp of 5 K/s. The corresponding TPD spectra are shown in part a of Figure 4 for the  $\sim 5$  nm Au NPs and in part a of Figure 5 for  $\sim 1.5$  nm Au NPs. In the case of the 1.5 nm Au NPs (sample #3), due to the small intensity of the  $\gamma$  peak ( $O_2$  desorption from gold) with respect to the substrate  $\sigma$  peak ( $O_2$  desorption from SiO<sub>2</sub>), as well as to the partial overlap of these two desorption features, the complete analysis method cannot be applied to the raw TPD data. For that reason our analysis is based on background subtracted data (single peak features in part a of Figure 5) of this sample. It should be noted that large errors are expected in the kinetic parameters obtained for the small NPs using the complete analysis method due to uncertainties in the choice of background.

Atomic oxygen coverage versus temperature plots obtained from the data shown in part a of Figure 4 (raw data) and in part a of Figure 5 (background subtracted data) are displayed in part b of Figure 4 and part b of Figure 5. The complete analysis method provides insight into the dependency of the activation

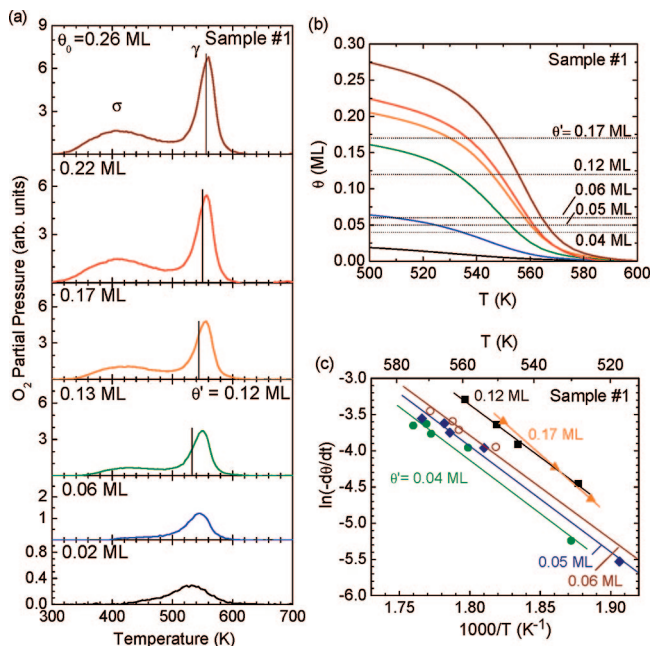


**Figure 4.** (a) Coverage-dependent O<sub>2</sub> TPD spectra obtained for a constant heating rate of 5 K/s on  $\sim 5$  nm Au NPs (sample #1) deposited on SiO<sub>2</sub>. From the integration of the individual TPD spectra and after appropriate normalization, oxygen coverages on gold of  $\theta_0$  0.02, 0.06, 0.13, 0.17, 0.22, and 0.26 ML (from bottom to top) were obtained. (b) Temperature-dependent evolution of the atomic oxygen coverage on gold (sample #1). (c) Arrhenius plot of  $\ln(-d\theta/dt)$  at different coverages  $\theta'$  (sample #1).

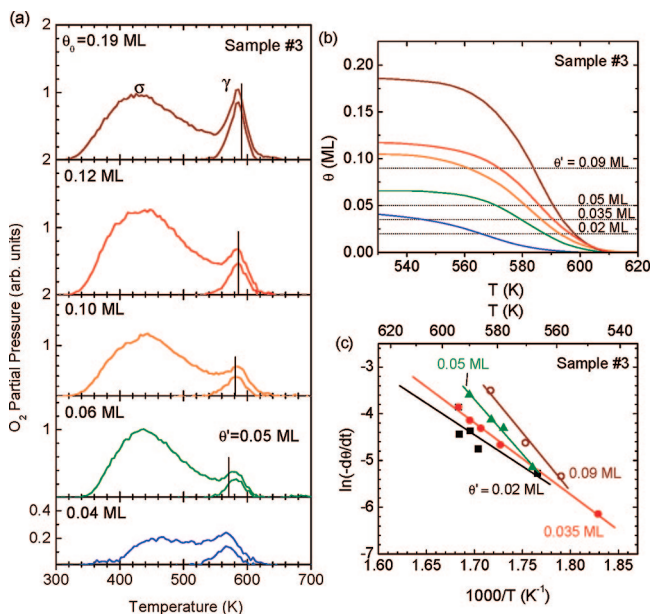


**Figure 5.** (a) Coverage-dependent O<sub>2</sub> TPD spectra obtained for a constant heating rate of 5 K/s on  $\sim 1.5$  nm Au NPs (sample #3) deposited on SiO<sub>2</sub>. From the integration of the individual TPD spectra and after appropriate normalization, oxygen coverages on gold of  $\theta_0$  0.04, 0.06, 0.10, 0.12, and 0.19 ML (from bottom to top) were obtained. (b) Temperature-dependent evolution of the atomic oxygen coverage on gold (sample #3). (c) Arrhenius plot of  $\ln(-d\theta/dt)$  at different coverages  $\theta'$  (sample #3).

energy and prefactor on the adsorbate coverage. In the complete analysis, a coverage  $\theta'$  is chosen ( $0 < \theta' < \theta_0$ ) for which the kinetic parameters are to be determined, and  $(-d\theta/dt, T)$  points corresponding to that fixed coverage are found in each TPD spectrum (marked by solid lines in part a of Figure 4 and in

part a of Figure 5). This procedure was repeated for several different values of  $\theta'$ , and for each of these, an Arrhenius plot of  $\ln(-d\theta/dt)$  versus  $1/T$  is made, as is shown in part c of Figure 4 and in part c of Figure 5. The slope of these curves yields the activation energy for desorption for that particular oxygen coverage [ $E_d(\theta')$ ], whereas the prefactor  $\nu_n(\theta')$  is obtained from the intercept with the y axis [ $\ln \nu_n(\theta') + n \ln \theta'$ ], after assuming a value for the desorption order.<sup>34</sup> The results from the complete analysis are compiled in Table 1. As an example, taking a coverage  $\theta' = 0.12$  ML and  $n = 1$ , a desorption energy of  $1.3 \pm 0.1$  eV and a pre-exponential factor  $6 \times 10^{10 \pm 1}$  s<sup>-1</sup> were obtained for our  $\sim 5$  nm NPs from the complete analysis. This result is in agreement with the data obtained from the HRV method and the derivative of the PW equation on sample #1 (1.2 eV and  $\sim 1 \times 10^{10}$  s<sup>-1</sup>). Repeating this analysis for different choices of  $\theta'$  leads to significant variations in the obtained values of the activation energy and the prefactor (Table 1), suggesting that the kinetic parameters of this process in fact depend on the adsorbate coverage. This result indicates that integral analysis methods such as the Redhead method will not properly describe the kinetics of this desorption process.

Using the complete analysis on the TPD data of the  $\sim 1.5$  nm NPs (sample #3), very large differences in the activation energies (1.2–2.2 eV) and second-order pre-exponential factors ( $10^{11}$  to  $10^{19}$  ML<sup>-1</sup> s<sup>-1</sup>) were obtained for different adsorbate coverages (0.02–0.09 ML), as shown in Table 1. The  $\nu_2$  values obtained for the largest  $\theta'$  coverages investigated are excessively high. Such large differences could have at least partially a physical origin (as for example interactions between mobile adsorbates) but might also be due to analysis artifacts originating from the overlap between gold and SiO<sub>2</sub> oxygen desorption features in this sample (#3). In fact, the subtraction of the SiO<sub>2</sub> background from the raw TPD spectra of this sample (single-peak features in part a of Figure 5) constitutes an additional source of error in the complete analysis. Artificial compensation effects could also explain the wide range of values of the pre-exponential factors and activation energies obtained on this system. The inherent complexity of the present nanoscale system prevents the assignment of these effects to a unique factor.

As was discussed in the analysis methods section, it is possible to extract the desorption order from a set of coverage-dependent O<sub>2</sub> TPD spectra.<sup>2,25</sup> The method is based on  $\ln(-d\theta/dt)$  versus  $\ln(\theta)$  plots conducted for a fixed temperature, in which the slope should yield the desorption order,  $n$ . Such plot for the 5 nm Au NPs (sample #1) is included in part a of Figure 6. From this graph, an apparent desorption order of  $n \sim 1$  was calculated for the large Au NPs. The plot in part a of Figure 6 corresponds to the following fixed temperatures: 561 K ( $n = 1.14 \pm 0.07$ ), 554 K ( $n = 1.01 \pm 0.07$ ), and 546 K ( $n = 0.89 \pm 0.07$ ). However, we would like to stress that this approximation is only valid if  $E_d$  and  $\nu_n$  do not depend on the coverage. A similar analysis was done based on desorption data from the small Au NPs, as shown in part b of Figure 6. Here, the following desorption orders were obtained at three given temperatures: 575 K ( $n = 0.54 \pm 0.06$ ), 585 K ( $n = 0.87 \pm 0.05$ ), and 595 K ( $n = 0.98 \pm 0.07$ ). The  $n$  values obtained here are nonphysical, suggesting that the last two terms in eq 6 must be significant. This could be an indirect proof of a strong coverage dependency of the kinetic parameters of O<sub>2</sub> desorption from small Au NPs supported on SiO<sub>2</sub>.

**c) Redhead Method.** As was mentioned in the analysis methods section, the Redhead method can be used to obtain the desorption energy of a reaction for a fixed adsorbate coverage, assuming that both the reaction order and the pre-

**TABLE 1: Summary of the Kinetic Parameters [Desorption Order, Desorption Energy and Pre-exponential Factor] Obtained from Our O<sub>2</sub> TPD Measurements on ~5 nm (Sample #1) and ~1.5 nm (Sample #3) Au Nanoparticles Deposited on SiO<sub>2</sub> Using Different Analysis Methods<sup>a</sup>**

| sample                          | analysis method      | desorption order ( <i>n</i> ) | desorption energy ( <i>E<sub>d</sub></i> )              | pre-exponential factor ( <i>ν<sub>n</sub></i> )         | comments   |
|---------------------------------|----------------------|-------------------------------|---|---|--|
| Au NPs ~5 nm/SiO <sub>2</sub>   | Arrhenius            |                               |   |   | no linear fit  |
|                                 | HRV                  | * <i>n</i> = 1                | 1.2 ± 0.1 eV  | 1 × 10 <sup>10±1</sup> s <sup>-1</sup>                  | θ <sub>0</sub> = 0.22 ML β = 0.1~5 K/s                             |
|                                 |                      | * <i>n</i> = 2                | 1.2 ± 0.1 eV  | 4 × 10 <sup>10±1</sup> ML <sup>-1</sup> s <sup>-1</sup> |  |
|                                 | Redhead              | * <i>n</i> = 1                | 1.5 eV  | *1 × 10 <sup>13</sup> s <sup>-1</sup>                   | θ <sub>0</sub> = 0.22 ML β = 5 K/s <i>T</i> <sub>max</sub> = 555 K |
|                                 |                      | * <i>n</i> = 2                | 1.4 eV  | *1 × 10 <sup>13</sup> ML <sup>-1</sup> s <sup>-1</sup>  |  |
|                                 | complete analysis    | * <i>n</i> = 1                | 1.3 ± 0.1 eV  | 1 × 10 <sup>11±1</sup> s <sup>-1</sup>                  | θ' = 0.04 ML β = 5 K/s   |
|                                 |                      |                               | 1.3 ± 0.1 eV  | 6 × 10 <sup>10±1</sup> s <sup>-1</sup>                  | θ' = 0.12 ML β = 5 K/s   |
|                                 |                      |                               | 1.5 ± 0.1 eV  | 6 × 10 <sup>12±1</sup> s <sup>-1</sup>                  | θ' = 0.17 ML β = 5 K/s   |
|                                 |                      | * <i>n</i> = 2                | 1.3 ± 0.1 eV  | 3 × 10 <sup>12±1</sup> ML <sup>-1</sup> s <sup>-1</sup> | θ' = 0.04 ML β = 5 K/s   |
|                                 |                      |                               | 1.3 ± 0.1 eV  | 5 × 10 <sup>11±1</sup> ML <sup>-1</sup> s <sup>-1</sup> | θ' = 0.12 ML β = 5 K/s   |
| 1.5 ± 0.1 eV                    |                      |                               | 4 × 10 <sup>13±1</sup> ML <sup>-1</sup> s <sup>-1</sup> | θ' = 0.17 ML β = 5 K/s                                  |  |
| ln(-dθ/dt) vs ln(θ)             | <i>n</i> = 1.0 ± 0.1 |                               |   | β = 5 K/s <i>T</i> <sub>max</sub> = 555 K               |  |
| Au NPs ~1.5 nm/SiO <sub>2</sub> | Arrhenius            | <i>n</i> = 2                  | 1.6 ± 0.1 eV  | 7 × 10 <sup>14±1</sup> ML <sup>-1</sup> s <sup>-1</sup> | θ <sub>0</sub> = 0.31 ML β = 5 K/s                                 |
|                                 | HRV                  | * <i>n</i> = 2                | 1.7 ± 0.1 eV  | 2 × 10 <sup>15±1</sup> ML <sup>-1</sup> s <sup>-1</sup> | θ <sub>0</sub> = 0.26 ML β = 0.7~5 K/s                             |
|                                 | Redhead              | * <i>n</i> = 2                | 1.5 eV  | *1 × 10 <sup>13</sup> ML <sup>-1</sup> s <sup>-1</sup>  | θ <sub>0</sub> = 0.26 ML β = 5 K/s <i>T</i> <sub>max</sub> = 584 K |
|                                 |                      | * <i>n</i> = 2                | 1.6 eV  | *1 × 10 <sup>14</sup> ML <sup>-1</sup> s <sup>-1</sup>  |  |
|                                 | complete analysis    | * <i>n</i> = 2                | 1.2 eV  | 3 × 10 <sup>11±1</sup> ML <sup>-1</sup> s <sup>-1</sup> | θ' = 0.02 ML β = 5 K/s   |
|                                 |                      |                               | 1.3 eV  | 3 × 10 <sup>12±1</sup> ML <sup>-1</sup> s <sup>-1</sup> | θ' = 0.035 ML β = 5 K/s  |
|                                 |                      | 2.0 eV                        | 2 × 10 <sup>18±1</sup> ML <sup>-1</sup> s <sup>-1</sup> | θ' = 0.05 ML β = 5 K/s                                  |  |
|                                 |                      | 2.2 eV                        | 1 × 10 <sup>19±1</sup> ML <sup>-1</sup> s <sup>-1</sup> | θ' = 0.09 ML β = 5 K/s                                  |  |
| simulation                      | * <i>n</i> = 2       | 1.7 eV                        | 1.2 × 10 <sup>14</sup> ML <sup>-1</sup> s <sup>-1</sup> | θ <sub>0</sub> = 0.31 ML β = 5 K/s                      |  |

<sup>a</sup> The values with \* indicate the assumptions made by each analysis method. θ indicates the relative O coverage on gold.

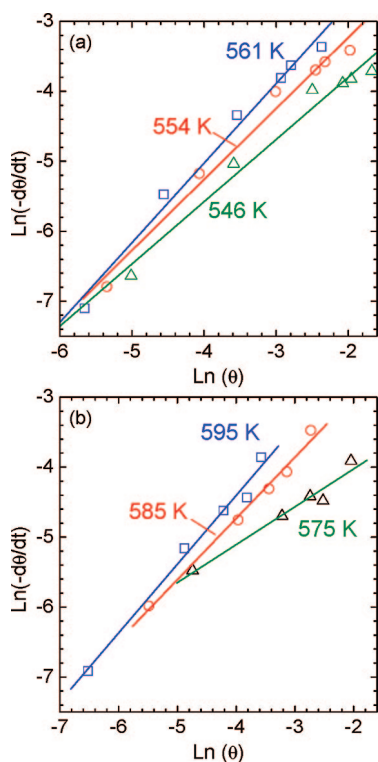


**Figure 6.** Plot of  $\ln(-d\theta/dt)$  vs  $\ln(\theta)$  for (a) ~5 nm large Au NPs on SiO<sub>2</sub> (sample #1) at the following constant temperatures: 561 K (squares), 554 K (circles), 546 K (triangles); and (b) ~1.5 nm (sample #3) at: 595 K (squares), 585 K (circles), 575 K (triangles). The fits indicate  $n \approx 1$  for the ~5 nm large Au NPs, and  $n$  between 0.5 and 1 for ~1.5 nm Au NPs.

exponential factor are known and independent of the coverage. From eq 2, and assuming  $n = 1$  and a pre-exponential factor of  $1 \times 10^{13} \text{ s}^{-1}$ ,  $E_d = 1.5 \text{ eV}$  for the ~5 nm gold clusters (sample #1). For the same sample, assuming  $n = 2$  and  $\nu_2 = 1 \times 10^{13} \text{ ML}^{-1} \text{ s}^{-1}$ , eq 3 leads to  $E_d = 1.4 \text{ eV}$ . For our small Au NPs

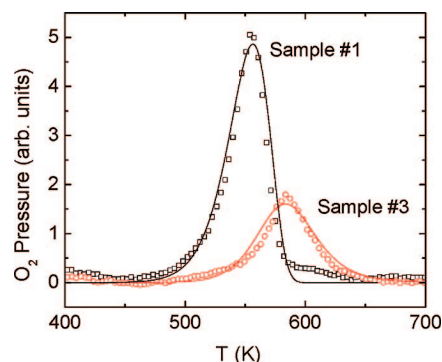


**Figure 7.** Numerical simulation of the PW equation (solid lines) on ~5 nm large Au NPs on SiO<sub>2</sub> (sample #1, θ<sub>0</sub> = 0.22 ML, squares) and ~1.5 nm Au NPs (sample #3, θ<sub>0</sub> = 0.31 ML, circles). The best fit was obtained for the following kinetic parameters:  $n = 1$ ,  $E_d = 1.5 \text{ eV}$  and  $\nu_1 = 1 \times 10^{13} \text{ s}^{-1}$  for sample #1, and  $n = 2$ ,  $E_d = 1.7 \text{ eV}$ , and  $\nu_2 = 1.2 \times 10^{14} \text{ ML}^{-1} \text{ s}^{-1}$  for sample #3.

(~1.5 nm), assuming  $n = 1$  and  $\nu_1 = 1 \times 10^{13} \text{ s}^{-1}$ ,  $E_d = 1.7 \text{ eV}$ . For the same sample, taking  $n = 2$  and  $\nu_2 = 1 \times 10^{13} \text{ ML}^{-1} \text{ s}^{-1}$ , a desorption energy of 1.5 eV was obtained. Again, the accuracy of these results is questionable, especially for the case of the small NPs because this method disregards the possible dependence of  $E_d$  and  $\nu_n$  on the coverage.

**d) Numerical Simulation of the PW Equation.** Figure 7 contains raw TPD spectra of oxygen desorption from ~5 nm large Au NPs on SiO<sub>2</sub> (sample #1, θ<sub>0</sub> = 0.22 ML, squares) and ~1.5 nm Au NPs (sample #3, θ<sub>0</sub> = 0.31 ML, circles) together with spectra simulated using the PW equation (solid lines) as shown in eq 1. The best fit to the experimental data was obtained for the following kinetic parameters:  $n = 1$ ,  $E_d = 1.5 \text{ eV}$  and  $\nu_1 = 1 \times 10^{13} \text{ s}^{-1}$  for sample #1, and  $n = 2$ ,  $E_d = 1.7 \text{ eV}$ , and  $\nu_2 = 1.2 \times 10^{14} \text{ ML}^{-1} \text{ s}^{-1}$  for sample #3. The simulations confirmed that the O<sub>2</sub> desorption from our large Au NPs can best be described by first-order kinetics, whereas a second-order kinetic equation was found to properly describe the TPD data obtained on the small NPs. For the large NPs, the values of the

kinetic parameters extracted from the simulations are in good agreement with the results obtained from the Redhead and complete analysis methods. In the case of the small NPs, our Arrhenius plots for a fixed coverage, the Redhead, and HRV methods provide results in accord with the simulations.

Strict quantitative analysis of our systems requires a more elaborated expression for the rate of desorption than the PW equation. Dynamic Monte Carlo simulations might be good candidates to improve our understanding of desorption processes at the molecular level.<sup>32,35–37</sup>

For comparison, we have included in Table 1 O<sub>2</sub> desorption kinetic parameters obtained from our experimental data on ~5 nm (sample #1) and ~1.5 nm (sample #3) gold nanoparticles deposited on SiO<sub>2</sub> using different methods: Arrhenius plots for a fixed initial adsorbate coverage (from ref 10), HRV,<sup>17</sup> complete analysis,<sup>16</sup> and the Redhead method.<sup>15</sup>

### Further Discussion

We would like to emphasize that the system under investigation here, namely supported nanometer-sized catalysts, is a complex system and complex reaction kinetics are expected. Therefore, care should be taken when comparing the kinetic parameters obtained from our TPD experiments to those previously reported on gold single-crystal surfaces. For example, different activation energies and pre-exponential factors have been reported in the literature for gold single crystals with different surface terminations,<sup>4,6–9,11,38</sup> and our faceted gold nanoparticles certainly include several of these orientations.

Our TPD results on large Au NPs (~5 nm) supported on SiO<sub>2</sub> are in closest agreement with the data obtained by Parker et al.<sup>5</sup> and Saliba et al.<sup>6</sup> after exposing a Au(111) surface to ozone ( $E_d = 1.24$  eV,  $\nu_1 = 2.7 \times 10^{11}$  s<sup>-1</sup> for  $\theta = 0.22$  ML). The similarity in the kinetic parameters obtained may be related to the presence of a (111) terrace on the top of Au NPs as observed in STM studies.<sup>38</sup> The O<sub>2</sub> TPD desorption peaks from Parker et al.<sup>5</sup> and Saliba et al.<sup>6</sup> were found to be asymmetric, resembling a first-order kinetic behavior over the entire coverage range (0.03–1.2 ML) under study.<sup>6</sup> For small coverages ( $\theta_0 = 0.03$  ML), a desorption energy and first-order frequency of 1.0 eV and  $5.5 \times 10^{11}$  s<sup>-1</sup> respectively were obtained, whereas for intermediate coverages ( $\theta_0 = 0.22$  ML) an increased  $E_d = 1.24$  eV and  $\nu_1 = 2.7 \times 10^{11}$  s<sup>-1</sup> were found.

Furthermore, good qualitative and quantitative agreement also exists between our TPD data and those obtained by Campbell's group on preoxidized gold islands deposited on TiO<sub>2</sub>(110).<sup>9</sup> Using the Redhead analysis method and assuming  $n = 1$  and  $\nu_1 = 5.5 \times 10^{12}$  s<sup>-1</sup>, they reported activation energies for O<sub>2</sub> desorption of 1.97 eV ( $T_{\max} = 741$  K), 1.71 eV ( $T_{\max} = 645$  K), and 1.44 eV ( $T_{\max} = 520$  K) for 1, 2, and 6 atom thick gold islands, respectively.<sup>9,39,40</sup> In analogy to our experimental data, the highest  $E_d$  was also found for the smallest gold islands investigated. It is important to note that our results were obtained on Au NPs deposited on SiO<sub>2</sub>, whereas the data from Campbell's group<sup>9</sup> were obtained on Au NPs supported on TiO<sub>2</sub>. Although nanoparticle-support interactions could in principle lead to indirect size-dependent changes in  $E_d$ , it seems unlikely that these would affect the desorption process identically on different substrates. We therefore conclude that the change in the activation energy detected on NPs of different average size is directly related to the NP size, and not to nanoparticle-support interactions.

### Conclusions

Heating rate- and coverage-dependent TPD experiments on gold NPs prepared by an inverse micelle method on SiO<sub>2</sub>

substrates yielded values of  $E_d = 1.3 \pm 0.2$  eV and  $\nu_1 = 10^{11 \pm 1}$  s<sup>-1</sup> (averaged from Table 1) for first-order desorption from large (~5 nm) Au NPs and  $E_d = 1.3 \pm 0.2$  eV and  $\nu_2 = 10^{12 \pm 1}$  ML<sup>-1</sup> s<sup>-1</sup> with the assumption of second-order desorption. The HRV and complete analysis methods provide similar results for coverages in the range 0.04–0.17 ML on ~5 nm Au NPs. The results obtained on ~1.5 nm Au NPs based on the HRV method ( $E_d = 1.7 \pm 0.1$  eV and  $\nu_2 \sim 2 \times 10^{15 \pm 1}$  ML<sup>-1</sup> s<sup>-1</sup>) are in good agreement with the values resulting from the Arrhenius plot of a single TPD spectrum shown in ref 10 ( $n = 2$ ,  $E_d = 1.6 \pm 0.1$  eV and  $\nu_2 = 7 \times 10^{14 \pm 1}$  ML<sup>-1</sup> s<sup>-1</sup>). However, scattered values of the kinetic parameters were obtained on this sample based on the complete analysis,  $E_d = 1.7 \pm 0.5$  eV and  $\nu_2 = 4 \times 10^{18 \pm 1}$  ML<sup>-1</sup> s<sup>-1</sup> (averaged from Table 1 for  $n = 2$ ), for coverages ranging from 0.02 to 0.09 ML. A careful review of the literature shows that, even for bulk gold, large variations in the prefactor and desorption energy were observed. Most of these variations can be attributed to the distinct analysis methods employed. Our data on the small Au NPs indicate that conventional TPD analysis models are only approximations that might not properly describe a system of the complexity of the one at hand.

Summarizing, independent of the analysis method used, our data provide evidence of clear size effects in the desorption of O<sub>2</sub> from supported Au NPs with higher activation energies detected on the smallest NPs investigated. Furthermore, the excellent agreement with previous data on gold clusters supported on a different oxide (TiO<sub>2</sub><sup>9,39</sup> versus SiO<sub>2</sub> in the present study) indicate that support effects are not responsible for the distinct activation energies obtained on nanoparticles with different average size.

**Acknowledgment.** We are thankful to Prof. Charles T. Campbell (Univ. Washington at Seattle), Prof. Werner Keune (Univ. Duisburg-Essen), and Prof. Pieter G. Kik (Univ. Central Florida) for stimulating discussions. Financial support from the National Science Foundation (NSF-CAREER award, 0448491) is greatly appreciated.

### References and Notes

- (1) Gottfried, J. M.; Schmidt, K. J.; Schroeder, S. L. M.; Christmann, K. *Surf. Sci.* **2002**, *511*, 65.
- (2) Gottfried, J. M.; Schmidt, K. J.; Schroeder, S. L. M.; Christmann, K. *Surf. Sci.* **2003**, *525*, 184.
- (3) Gottfried, J. M.; Elghobashi, N.; Schroeder, S. L. M.; Christmann, K. *Surf. Sci.* **2003**, *523*, 89.
- (4) Sault, A. G.; Madix, R. J.; Campbell, C. T. *Surf. Sci.* **1986**, *169*, 347.
- (5) Parker, D. H.; Koel, B. E. *J. Vac. Sci. Technol. A* **1990**, *8*, 2585.
- (6) Saliba, N.; Parker, D. H.; Koel, B. E. *Surf. Sci.* **1998**, *410*, 270.
- (7) Kim, J.; Samano, E.; Koel, B. E. *Surf. Sci.* **2006**, *600*, 4622.
- (8) Deng, X. Y.; Min, B. K.; Guloy, A.; Friend, C. M. *J. Am. Chem. Soc.* **2005**, *127*, 9267.
- (9) Bondzie, V. A.; Parker, S. C.; Campbell, C. T. *J. Vac. Sci. Technol., A* **1999**, *17*, 1717.
- (10) Ono, L. K.; Roldan Cuenya, B. *J. Phys. Chem. C* **2008**, *112*, 4676.
- (11) Choi, K. H.; Coh, B. Y.; Lee, H. I. *Catal. Today* **1998**, *44*, 205.
- (12) Ono, L. K.; Sudfeld, D.; Roldan Cuenya, B. *Surf. Sci.* **2006**, *600*, 5041.
- (13) Chan, C. M.; Aris, R.; Weinberg, W. H. *Appl. Surf. Sci.* **1978**, *1*, 360.
- (14) Taylor, J. L.; Weinberg, W. H. *Surf. Sci.* **1978**, *78*, 259.
- (15) Redhead, P. A. *Vacuum* **1962**, *12*, 203.
- (16) King, D. A. *Surf. Sci.* **1975**, *47*, 384.
- (17) Falconer, J. L.; Madix, R. J. *Surf. Sci.* **1975**, *48*, 393.
- (18) Polanyi, M.; Wigner, E. Z. *Phys. Chem.* **1928**, *139*, 439.
- (19) Hickmott, T. W.; Ehrlich, G. *J. Phys. Chem. Sol.* **1958**, *5*, 47.
- (20) Miller, J. B.; Siddiqui, H. R.; Gates, S. M.; Russell, J. N.; Yates, J. T.; Tully, J. C.; Cardillo, M. J. *J. Chem. Phys.* **1987**, *87*, 6725.
- (21) Habenschaden, E.; Kupperts, J. *Surf. Sci.* **1984**, *138*, L147.

- (22) King, D. A.; Madey, T. E.; Yates, J. T. *J. Chem. Phys.* **1971**, *55*, 3236.
- (23) Niemantsverdriet, J. W.; Markert, K.; Wandelt, K. *Appl. Surf. Sci.* **1988**, *31*, 211.
- (24) Ibbotson, D. E.; Wittrig, T. S.; Weinberg, W. H. *J. Chem. Phys.* **1980**, *72*, 4885.
- (25) Wittrig, T. S.; Ibbotson, D. E.; Weinberg, W. H. *Appl. Surf. Sci.* **1980**, *4*, 234.
- (26) Bond, G. C.; Keane, M. A.; Kral, H.; Lercher, J. A. *Catal. Rev.* **2000**, *42*, 323.
- (27) Nieskens, D. L. S.; van Bavel, A. P.; Niemantsverdriet, J. W. *Surf. Sci.* **2003**, *546*, 159.
- (28) de Jong, A. M.; Niemantsverdriet, J. W. *Surf. Sci.* **1990**, *233*, 355.
- (29) Niemantsverdriet, J. W.; Wandelt, K. *J. Vac. Sci. Technol., A* **1988**, *6*, 757.
- (30) Niemantsverdriet, J. W. *Spectroscopy in Catalysis - An Introduction*; VCH Verlagsgesellschaft mbH: Weinheim, 1993.
- (31) Ono, L. K.; Roldan Cuenya, B. *J. Phys. Chem. C*, 2008 (reply to comment, in press).
- (32) Zhdanov, V. P.; Kasemo, B. *Surf. Sci.* **1998**, *405*, 27.
- (33) Roldan Cuenya, B.; Naitabdi, A.; Croy, J.; Sturhahn, W.; Zhao, J. Y.; Alp, E. E.; Meyer, R.; Sudfeld, D.; Schuster, E.; Keune, W. *Phys. Rev. B* **2007**, *76*, 195422.
- (34) In principle, the desorption order,  $n$ , can also be extracted from the complete analysis through a  $[\ln v_d(\theta') + n \ln \theta']$  versus  $[\ln \theta']$  plot, provided that a linear dependency is observed. Unfortunately, both of our samples showed scattered intercept data, preventing such analysis over the range of oxygen coverages investigated here.
- (35) van Bavel, A. P.; Curulla Ferre, D.; Niemantsverdriet, J. W. *Chem. Phys. Lett.* **2005**, *407*, 227.
- (36) Jansen, A. P. *J. Phys. Rev. B* **2004**, *69*, 035414.
- (37) Myyrylainen, M.; Rantala, T. T. *Catal. Today* **2005**, *100*, 413.
- (38) Barke, I.; Hovel, H. *Phys. Rev. Lett.* **2003**, *90*, 166801.
- (39) Bondzie, V. A.; Parker, S. C.; Campbell, C. T. *Catal. Lett.* **1999**, *63*, 143.
- (40) The correct  $E_d$  in refs 9 and 40 are: 1.44, 1.70, and 1.97 eV for 6, 2, and 1 atom thick gold islands, respectively. See Errata to ref 9 and by C.T. Campbell in *J. Vac. Sci. Tech. A*, 2008, and *Catal. Lett.*, 2008, in press.

JP8065184